

Azimuthal patterns in planetesimal circumstellar disks

Tatiana Demidova^{1,2*}, Ivan Shevchenko^{2,3}

¹ *Crimean Astrophysical Observatory RAS, Nauchniy*

² *St. Petersburg State University, Universitetskaya emb. 7/9, 199034 St. Petersburg*

³ *Institute of Applied Astronomy RAS, nab. Kutuzova 10, 191187 St. Petersburg*

Abstract. Ways of formation of azimuthal resonant patterns in circumstellar planetesimal disks with planets are considered. Our analytical estimates and massive numerical experiments show that the disk particles that initially reside in zones of low-order mean-motion resonances with the planet may eventually concentrate into potentially observable azimuthal patterns. The structuring process is rapid, usually taking ~ 100 orbital periods of the planet. It is found that the relative number of particles that retain their resonant position increases with decreasing the mass parameter μ (the ratio of masses of the perturbing planet and the parent star), but a significant fraction of the particle population is always removed from the disk due to accretion of the particles onto the star and planet, as well as due to their transition to highly elongated and hyperbolic orbits. Expected radio images of azimuthally structured disks are constructed. In the considered models, azimuthal patterns associated with the 2:1 and 3:2 resonances are most clearly manifested; observational manifestations of the 1:2 and 2:3 resonances are also possible.

Keywords: mean-motion resonances, dynamical chaos, debris disks, planetesimal disks, planetesimals.

*e-mail: <proxima1@list.ru>

Introduction

Presence of planets in a debris planetesimal disk has a significant effect on the low-mass matter distribution inside the disk. Mean-motion resonances with a planet form ring-shaped dense structures as well as matter-free cavities in the disk [Ozernoy et al., 2000, Quillen and Thorndike, 2002, Kuchner and Holman, 2003, Quillen and Faber, 2006, Mustill and Wyatt, 2012, Morrison and Malhotra, 2015, Demidova and Shevchenko, 2016]. Planetary perturbations can form the disk boundaries, both external and internal, depending on the system configuration [Wyatt et al., 1999, Quillen, 2006, Su et al., 2013, Rodigas et al., 2014].

The planetesimal (debris) circumstellar disk is formed together with the planetary system of a star as a result of the evolution of the protoplanetary gas-dust disk [see, e.g., the review by Marino, 2022]. The debris disk consists of solid bodies with sizes in a broad range, from fine micron-sized dust to kilometer-sized and larger planetesimals.

Previously, we considered the formation of spiral and ring patterns in debris disks [Demidova and Shevchenko, 2015, 2016]. Here we study an *azimuthal* structuring by the planet of the debris disk matter that occur in the vicinities of resonances of mean motions (mean orbital frequencies) of minor bodies with the planet [Murray and Dermott, 2000, Shevchenko, 2020]. We consider first-order resonances, namely, the 2:1, 3:2, 1:2, and 2:3 ones.

Formation of resonant azimuthal patterns

Note that, according to Kondratyev [2014], the circumstellar disk surface density distribution, which consists of many Keplerian orbits, may have maxima near the inner and outer boundaries of the disk. The density maximum at the inner boundary is due to the crowding of orbits near the pericenters. A similar density thickening can be seen in the initial distribution of particles in Fig. 1. Emergence of the maximum at the apocenter is due to the particle dynamics, and therefore does not manifest itself in the particle initial distribution.

It is known that the velocity of a body in an elliptical orbit is maximum at the orbit pericenter and minimum at the apocenter. The velocity values are, respectively, given by

$$v_p = na\sqrt{\frac{1+e}{1-e}}, \quad v_a = na\sqrt{\frac{1-e}{1+e}}, \quad (1)$$

where n , a , and e are the orbital mean motion, semimajor axis, and eccentricity, respectively; see, e. g., formulas (2.35) in Murray and Dermott [2000]. Therefore, the ratio of the maximum and minimum velocities is

$$v_p/v_a = \frac{1+e}{1-e}, \quad (2)$$

and, accordingly, the ratio of the particle residence times in the vicinities of the apocenter and pericenter is

$$T_a/T_p \approx \frac{1+e}{1-e}, \quad (3)$$

which tends to infinity at $e \rightarrow 1$.

Planetary perturbations affect the particle surface density distribution. Our calculations show that the area at the disk’s inner boundary is cleared from matter.

Therefore, an external observer of an ensemble of particles in elongated orbits would see the particles mostly concentrated towards their orbital apocenters. This simple fact, as shown below, substantiates the opportunity for observational manifestation of azimuthal patterns in the disk.

In what follows, we assume that any mutual perturbations of particles in orbits are absent.

We consider the trajectories of particles in various resonances in a rotating (with the angular velocity of the perturbing planet) coordinate system. The planet’s orbit is assumed to be circular. Let us consider internal and external resonances of the first order.

If the particle resides in an internal $p + q : p$ resonance with the planet, then the “star–planet–particle” configuration is repeated on the time intervals equal to $p + q$ particle’s orbital periods; if the particle resides in an external $p : p + q$ resonance, then the configuration is repeated on the time intervals equal to p particle’s orbital periods [Murray and Dermott, 2000].

In Murray and Dermott [2000], particle trajectories are shown for some first-order resonances with the planet; see Fig. 8.4 in that book. In a rotating (with the planet’s angular velocity) coordinate system, the particle trajectories possess specific features, namely, loops, which appear either near the apocenter (for inner particles) or near the pericenter (for outer particles).

For the “star–planet–particle” configuration be once again repeated, at the $p + q : p$ internal resonance the particle should accomplish $p + q$ orbital revolutions, and, at the $p : p + q$ external resonance, p revolutions; therefore, the number of loops of its trajectory would be, respectively, $p + q$ and p .

The angular velocity of a planet in a circular orbit is constant, while that of a particle in an elliptical orbit varies with time. If, starting from zero, one increases the eccentricity of an inner particle’s orbit, then, at some critical eccentricity value, the particle’s angular velocity at the apocenter will coincide with the constant angular velocity of the planet, and, in the rotating coordinate system, the particle trajectory will acquire a cusp. If the eccentricity is increased further on, then the particle trajectory forms a backward loop.

It is straightforward to show [see Murray and Dermott, 2000] that for an inner particle in the $p + q : p$ resonance with the planet the cusp appears when its eccentricity e satisfies the cubic equation

$$(1 + e)^3 = [(p + q)/p]^2(1 - e), \quad (4)$$

and, for an external particle in the $p : p + q$ resonance with the planet, it appears at e' satisfying the cubic equation

$$(1 - e')^3 = [p/(p + q)]^2(1 + e'). \quad (5)$$

For example, solving the Eq. (4) for the 2:1, 3:2, and 4:3 internal resonances gives the critical values of e equal to 0.365, 0.211 and 0.148, respectively [Murray and Dermott, 2000].

According to the Eq. (3), the maximum contrast in the observed apocentric and pericentric concentrations of particles should be expected in the first of these cases (resonance 2:1), and the minimum contrast is in the third case (resonance 4:3).

In the Solar system, an actual example of a resonant group, forming a weakly pronounced quasi-triangular rotating (with the angular velocity of Jupiter) pattern in the main asteroid belt, is provided by the Hilda group [L’vov et al., 2004], which resides in the 3:2 resonance with Jupiter.

The model and methods

Let us consider the disk dynamics in the planar problem in the barycentric frame. Let the system include a central star with mass $M = M_{\odot}$, a planet with mass m in a

circular orbit with period P and semimajor axis a , and a disk of passively gravitating particles, the parameters of which will be specified below.

Initially, the star is situated at the point with coordinates $(x, y) = (p_1, 0)$, and the planet is at the point $(p_2, 0)$, where $p_1 = -\frac{m}{M+m}a$ and $p_2 = \frac{M}{M+m}a$. The velocity vectors of the star and the planet initially have components $(0, -\frac{m}{M+m}na)$ and $(0, \frac{M}{M+m}na)$, respectively, where the mean motion $n = \frac{2\pi}{P}$. The model mass parameter $\mu = \frac{m}{M+m}$ is varied: the system dynamics is considered at its four values: $\lg \mu = -2, -3, -4$ and -5 .

Initially, 10^6 massless (passively gravitating) particles are placed at a given resonance. In [Demidova and Shevchenko, 2020], radial sizes of the ring-like chaotic zones at mean-motion resonances were estimated in dependence on the mass parameter: $\Delta a_r = 0.91\mu^{0.43}a$ for internal (with respect to the planet’s orbit) resonances, and $\Delta a_r = 1.32\mu^{0.42}a$ for external ones. Here we use these Δa_r values to determine the boundaries for the initial values of the semimajor axes of particle orbits: the particles are initially distributed randomly along the semimajor axis within $a_r \pm \frac{\Delta a_r}{2}$, where a_r is the resonance location. This choice of the boundaries is called forth by the fact that the particles are effectively ejected from the chaotic zone (where their concentration decreases with time, see Demidova and Shevchenko 2020), and thus can participate in formation of patterns.

There are also cosmogonic reasons for such a choice: if any planet in the disk were originally formed close to resonance with another planet and were destroyed by colliding with another object, e. g. planetary embryo (on collisional evolution during the formation stages of planetary systems, see Agnor et al. [1999], Chambers and Wetherill [1998], Taylor [1998]), this would contribute to an increase in the concentration of planetesimals in the resonance zone.

The calculations were performed for four mean-motion particle–planet resonances: two outer ones, 1:2 and 2:3, and two inner ones, 2:1 and 3:2. The initial eccentricities of particles are distributed randomly in the range $[0 : 1)$, and the initial true anomaly and longitude of pericenter values are randomly distributed in the range $[0, 2\pi)$.

The calculations were performed in the planar problem in rectangular barycentric frames. The planet and particles move in their orbits counterclockwise. The integration of the particle motion equations was carried out using the Bulirsch–Stoer algorithm [Stoer and Bulirsch, 1980, Press et al., 1992]. The error tolerance ϵ was set equal to 10^{-14} .

In the course of calculations, the Jacobi integral conservation was controlled for each particle. The method implementation is described in detail in Demidova [2022].

The disk particles may escape from the system due to three basic processes: accretion onto the planet, accretion onto the star, and scattering to an elongated orbit. The accretion radius for the star was set as $R_{\text{sa}} = 0.01 \left(\frac{M}{3m} \right)^{\frac{1}{3}} a$ and that for the planet as $R_{\text{pa}} = 0.01 \left(\frac{m}{3M} \right)^{\frac{1}{3}} a$. Any particles that approached the star or the planet within a distance less than the corresponding accretion radius were considered to have been accreted and were removed from the system. Any particles that moved away from the barycenter to a distance of more than 4 orbital radii of the planet were also regarded as escaped from the system. The maximum duration of integration of any particle orbit was set to 10^5 orbital periods of the planet.

In this study, the self-gravity of the planetesimal disk was not taken into account. Beust et al. [2014] and Pearce and Wyatt [2014] showed that the influence of a massive planet dominates over the mutual gravitational interactions of planetesimals if the planet’s mass is an order of magnitude (or more) greater than the disk’s mass. The planet’s minimum mass that we considered in this study is equal to $10^{-5} M_{\odot}$ (~ 3 Earth masses), and, for the planetesimals, only a ring of matter close to resonance was considered. Such a planet’s mass is an order of magnitude greater than the mass of the Kuiper belt and several orders of magnitude greater than the mass of the main asteroid belt, estimated in [Pitjeva and Pitjev, 2018a,b]. On this reason we assume that disk’s self-gravity can be neglected.

Particle dynamics

As soon as the distribution of particles and the rates of their removal from the system at all considered values of μ are respectively similar, solely the case of $\lg \mu = -3$, unless otherwise indicated, will be described in detail in what follows.

Particle distributions

Fig. 1 shows the initial distribution of particles in each model. Initially, the matter is concentrated in a ring where the corresponding resonance is located.

Due to planetary perturbations, the particle distribution acquires azimuthal patterns. Fig. 2 shows the particle distribution at the end of simulation, at time $t = 10^5 P$ (where P

is the planet’s orbital period). At the 1:2 resonance (Fig. 2, upper-left), a dense ring near the resonance location at $R \approx 1.58a$ (where a is the planet’s orbital radius) is preserved, but this ring-like pattern is already asymmetric: the particles condense behind the planet in the x axis, in its positive part. An area inside the ring becomes rarefied; asymmetric zones of reduced particle density are noticeable near the star and the planet. In addition, an arc-like region of reduced density emerges near $R = 2.4a$ (i. e., near the 2:7 resonance), located symmetrically with respect to the negative part of the x axis; the outer edge of the disk is asymmetric.

If the particles are initially distributed near the 2:3 resonance (Fig. 2, upper-right), the resulting annular pattern has two symmetric clusters along the y axis. Besides, near the y axis, two arc-like regions with reduced density emerge at $R \approx 2.08a$, corresponding to the 1:3 resonance. In the inner (with respect to the resonance location) zone, the matter is rarefied, and two symmetric cavities emerge, one near the planet and one on the opposite part of the x axis.

Near the 2:1 resonance (Fig. 2, lower-right), the symmetric ring is preserved. The matter in close-to-star space is rarefied. Besides, two cavities emerge, one near the planet, and a symmetric one on the opposite part of the x axis, as we have already seen in the 2:3 resonance case.

The most interesting azimuthal pattern emerges if the matter is initially distributed near the 3:2 resonance. The pattern has three matter condensations; and cavities are also formed: one of them surrounds the planet, and the other two are azimuthally displaced with respect to the planet by $\pm 120^\circ$. The matter in close-to-star space is also rarefied, as observed already in the previous cases.

Our computations show that the disk becomes structured on the time scale $\sim 100P$, and afterwards the picture changes with time only marginally.

Escaping particles

The time dependences of the number of escaping (leaving the system) particles manifest themselves similarly in all three basic processes of escape: in the beginning, a sharp increase in the number of escaping particles is observed, and afterwards the dependence eventually reaches a horizontal plateau. In the processes of accretion onto the planet and

scattering to distant orbits, the plateau is reached at time $\sim 400P$; whereas in the processes of accretion onto the star and transition to hyperbolic orbits, at $\sim 200P$. Thus, in the efficiency of particle removal, the first two processes substantially dominate.

In what concerns accretion onto the planet, mostly particles from the 3:2 and 2:3 resonance zones accrete, since these resonances are close to the planet’s orbit; particles from the internal resonance 3:2 are falling onto the planet much more often than those from the external resonance 2:3. Particles that are initially located near the 1:2 and 2:1 resonances provide approximately similar contributions to the accretion onto the planet (Fig. 3, upper-left).

In the process of accretion onto the star, particles from internal resonances dominate, but for the 2:1 and 2:3 resonances the difference is minor. Here, as in the case of accretion onto the planet, the 3:2 resonance particles dominate (Fig. 3, upper-right).

In the process of scattering to distant orbits, noticeably those particles mostly contribute that are initially located near external resonances, as one would expect. The dependences for the 1:2 and 2:3 resonances are very similar. Particles from the 3:2 resonance zone also substantially contribute to this scattering process (Fig. 3, lower-left).

Approximately 10% of particles that have crossed the $R = 4a$ limit are transferred to hyperbolic orbits, and can be therefore regarded as ejected from the system. Particles from the 1:2, 2:3, and 3:2 resonance zones contribute almost similarly to this process, whereas in the 2:1 resonance case the relative number of particles ejected to hyperbolic orbits is much less; see Fig. 3, lower-right panel.

Fig. 4 presents the number of particles that have left the system, as summed at the end of computation, in all our models. It can be seen that the number of particles accreting onto the planet, scattering to distant orbits, and passing to hyperbolic orbits increases with increasing the mass parameter μ . Conversely, in the case of accretion onto the star, the observed dependence is opposite; apparently, this is determined by an increase in the number of particles leaving the computation domain in other ways. Note that the relative number of particles that have left the computation domain in each of the processes coincides with that presented above in Fig. 3. Also note that for the minimum used here mass parameter value, namely $\lg \mu = -5$, the particles are not transferred to hyperbolic orbits in all considered resonance cases.

Observability of azimuthal patterns

The most interesting pattern that is observed in the final particle distribution has been obtained for the particles initially distributed near the 3:2 resonance. Fig. 5 presents the final distributions in four models with various values of the mass parameter μ . One may see that at $\lg \mu = -2$ the resulting pattern is strongly blurred, whereas at $\lg \mu = -3$ it clearly appears as a quasi-triangular one. On decreasing μ , the regions of increased particle density expand in azimuth, while the sizes of cavities decrease. Therefore, in what follows we concentrate on the possibility of actual astronomical observations of such a pattern when $\lg \mu = -3$.

Calculation of theoretical images

Sizes of particles in planetesimal disks vary from tens of micrometers to hundreds of kilometers [Wyatt, 2008, Krivov, 2010]. The size distribution is controlled by the process of destructive collisions of planetesimals; and the fine dust ($< 10\mu\text{m}$) is removed from the disk by radiation pressure [Krivov et al., 2000]. The collisional dynamics of planetesimals was studied in a number of papers [Dominik and Decin, 2003, Krivov et al., 2006, Wyatt et al., 2007, Thébault and Augereau, 2007, Löhne et al., 2008, Gáspár et al., 2012]. In particular, it was shown that the collisional evolution of particles leads to their size distribution in the form $dN = D^{2-3q}dD$ (where $q = 5/3 - 2$); and the mass distribution is $dN = m^{-q}dm$. Usually, in modeling, $q = 11/6$ is chosen:

$$dN = D^{-3.5}dD. \quad (6)$$

This q value is provided in the infinite collisional cascade model [Dohnanyi, 1969].

Then the mass fraction of particles of size D depends on D as follows: $dm \propto D^{-0.5}dD$. Integrating this relation, one finds that for the objects ranging in size from 100 km to 1 km the total contribution to the disk mass is $\sim 90\%$. However, thermal radiation in the submillimeter range, which can be detected by the ALMA (Atacama Large Millimeter Array) radio interferometer, is emitted by 0.1–10 mm particles [Marino, 2022].

Greaves [2005], Thébault and Augereau [2007] give estimates of mass of the dust ($D \leq 1$ cm) component in the typical debris disk: $M_{\text{dust}} = 0.001\text{--}0.1M_{\oplus}$. In our calculations for the emission of debris disk particles located in the resonance region, the fine

dust mass M_{dust} acts as a parameter of the problem. Three types of particles (with sizes 100 μm , 1 mm, and 1 cm) are considered. Mass M_{dust} is distributed between them according to Eq. (6). The mass of one particle of each type in our calculations is determined as follows: $m_{\text{D}} = M_{\text{dust}}/N_{\text{tot}} \cdot f_{\text{D}}$, where N_{tot} is the total number of disk particles at time $10^5 P$, and f_{D} is the relative fraction of particles of size D .

In the calculations of particle dynamics, we consider the planar (two-dimensional) problem; accordingly, in the radiation calculations, each particle is assigned with a random value of the coordinate z in the range $[-0.005 \text{ au}; 0.005 \text{ au}]$. Our calculations show that variations in the choice of the range in z do not significantly affect the general character of the emission of the structured disk.

The entire domain of computation is divided into cells in the spherical coordinate system, namely, $R \times \theta \times \phi = 200 \times 4 \times 90$, where $R \in [0.1a : 4a]$, $\theta \in [88^\circ.85 : 91^\circ.15]$, $\phi \in [0 : 2\pi)$. In each cell, the number of computed particles is summed (N_i), then the concentration of particles of each type in each cell is calculated:

$$\rho_{\text{d}} = \frac{m_{\text{D}} \cdot N_i}{R^2 \sin(\theta) dR d\theta d\phi}.$$

In our three-dimensional computations of radiative transfer we used the RADMC-3D code¹ [Dullemond et al., 2012]. The number of photons in the computations of the direct radiation and scattering was set to 10^9 . The dust opacity for magnesium–iron silicates [Dorschner et al., 1995] was calculated in the Mie theory [Mie, 1908], using the code by [Bohren and Huffman, 1998]; the RADMC-3D package includes this code.

We used the calculated radiation fluxes for construction of model images that can be potentially built using the ALMA radio interferometer. The simulation was performed using the CASA 6.5 simulator² [Petty and CASA Development Team, 2012] for the reference nominal (arbitrary) position ($\alpha = 04\text{h}33\text{m}$, $\delta = +22^\circ53'$, J2000), by analogy with the work by Ruge et al. [2015]. Thermal noise was added using the *tsys-atm* option of the CASA package, with the water vapour deposited at $PWV = 0.6$. It is assumed that the observations are performed at the wavelength $870\mu\text{m}$. The bandwidth for observations in the continuum was set equal to 8 GHz, the exposure time to 5 hr. The antenna configuration corresponds to the largest compact configuration (#20 of the available CASA

¹<https://www.ita.uni-heidelberg.de/dullemond/software/radmc-3d/>

²<https://casa.nrao.edu/>

configurations).

Image analysis

In our calculations of images of debris disk patterns, the input parameters were as follows: mass M_{dust} of fine (≤ 1 cm) dust, semimajor axis a of the planet’s orbit, and the distance d to the object. Fig. 6 presents a model with $M_{\text{dust}} = 0.001M_{\oplus}$, $a = 1$ AU, and $d = 10$ pc. The image obtained in the simulation looks blurred, but the bright zone has a definite quasi-triangular shape.

Consequent series of images was obtained in the model with $a = 5$ AU and $d = 10$ pc, while mass M_{dust} is varied (Fig. 7). One may see that, in the case of small $M_{\text{dust}} \leq 0.0005M_{\oplus}$, the pattern is resolved against the background noise, but it looks ragged; essentially, it forms an annular density perturbation. On increasing M_{dust} , three bright spots emerge in the image (they correspond to areas of increased density near the 3:2 resonance), and the disk pattern acquires a characteristic quasi-triangular shape.

Replacing the object to a greater distance d from the observer reduces the image resolution; however, even at $d = 20$ pc, the three bright spots corresponding to the disk matter clumps are still quite distinguishable if $M_{\text{dust}} \geq 0.001M_{\oplus}$ (Fig. 8, upper panels). When the object is replaced to 50 pc, the quasi-triangular pattern is distinguishable at $M_{\text{dust}} = 0.003M_{\oplus}$ (Fig. 8, lower panels) and would be more clear-cut at larger M_{dust} .

Conclusions

Our calculations showed that the disk particles, initially placed in zones of low-order mean-motion resonances with the planet, eventually concentrate into noticeable azimuthal patterns formed by thickening and cavities in the disk. In all considered models, the low-density cavities emerge close to the star and the planet. The structuring process usually proceeds on the time scale ~ 100 , in units of the planet orbital periods. The number of particles that retain their locations near the resonances increases with decreasing the mass parameter μ .

However, in all models, a removal of a significant fraction of particles from the disk is substantial due to their accretion onto the star and the planet, as well as due to transition to highly elongated and hyperbolic orbits. Particles can be transferred to hyperbolic orbits from the zones of all considered resonances, if $\lg \mu > -5$.

In the considered models, the azimuthal pattern associated with the 3:2 resonance manifests itself most clearly (if one sets $\lg \mu = -3$, corresponding to the mass ratio in the “Sun–Jupiter” system). Observability of such a pattern is real solely for the stars in the nearest Galactic neighborhood of the Sun; if $a > 5$ AU and $d > 50$ pc, the observability requires presence of fine dust of significant mass in the disk. However, it should be noted that the value of the mass M_{dust} accepted by us in the calculations does not exceed 3% of the maximum possible mass of fine dust in the debris disk.

Our simulations also revealed an azimuthal pattern associated with another considered first-order resonance, namely, the 2:1 resonance. Visual examples of actually observed azimuthal patterns, similar to those produced by this resonance, are provided by the protoplanetary circumstellar disks of the stars HD 169142 [Fedele et al., 2017], HD 97804 [van der Plas et al., 2017], and AA Tau [Loomis et al., 2017]; see also Fig. 1 in the review [Andrews et al., 2018]. Their possible correspondence with theoretical resonance models deserves separate analysis.

If one succeeds in the future to identify the presented above theoretical azimuthal patterns in the observed images of circumstellar disks, then, by modeling the image in each case, it would be possible to estimate the mass parameter μ and the orbital semimajor axis a of the planet that retains the particles in the resonance zone. For example, if a quasi-triangular bright pattern is detected in the image, the mass parameter μ can be estimated, based on results of our constructing the model images, as $\gtrsim 10^{-3}$, and the semimajor axis of the planet’s orbit $a \approx \left(\frac{3}{2}\right)^{\frac{2}{3}} a_t \approx 1.3a_t$, where a_t corresponds to radial location of the centers of the bright patterns.

Acknowledgments

The computations were carried out using the resources of the Joint Supercomputer Center of the Russian Academy of Sciences — Branch of Federal State Institution “Scientific Research Institute for System Analysis of the Russian Academy of Sciences”³ [Savin et al., 2019]. The study was supported by the Russian Foundation for Basic Research, project No. 22-22-00046.

³<https://www.jbcc.ru/>

References

- Craig B. Agnor, Robin M. Canup, and Harold F. Levison. On the Character and Consequences of Large Impacts in the Late Stage of Terrestrial Planet Formation. *Icarus*, 142(1):219–237, November 1999. doi: 10.1006/icar.1999.6201.
- S. M. Andrews, D. J. Wilner, E. Macías, C. Carrasco-González, and A. Isella. Resolved Substructures in Protoplanetary Disks with the ngVLA. In Eric Murphy, editor, *Science with a Next Generation Very Large Array*, volume 517 of *Astronomical Society of the Pacific Conference Series*, page 137, December 2018.
- H. Beust, J. C. Augereau, A. Bonsor, J. R. Graham, P. Kalas, J. Lebreton, A. M. Lagrange, S. Ertel, V. Faramaz, and P. Thébault. An independent determination of Fomalhaut b’s orbit and the dynamical effects on the outer dust belt. *Astron. Astrophys.*, 561:A43, January 2014. doi: 10.1051/0004-6361/201322229.
- Craig F. Bohren and Donald R. Huffman. *Absorption and Scattering of Light by Small Particles*. 1998.
- J. E. Chambers and G. W. Wetherill. Making the Terrestrial Planets: N-Body Integrations of Planetary Embryos in Three Dimensions. *Icarus*, 136(2):304–327, December 1998. doi: 10.1006/icar.1998.6007.
- T. Demidova. Bulirsh-Stoer algorithm in the planar restricted three-body problem. *Astronomy and Computing*, 41:100635, October 2022. doi: 10.1016/j.ascom.2022.100635.
- T. V. Demidova and I. I. Shevchenko. Three-lane and multilane signatures of planets in planetesimal discs. *Mon. Not. Roy. Astron. Soc.*, 463(1):L22–L25, November 2016. doi: 10.1093/mnrasl/slw150.
- T. V. Demidova and I. I. Shevchenko. Long-Term Dynamics of Planetesimals in Planetary Chaotic Zones. *Astronomy Letters*, 46(11):774–782, November 2020. doi: 10.1134/S1063773720100059.
- Tatiana V. Demidova and Ivan I. Shevchenko. Spiral Patterns in Planetesimal Circumbinary Disks. *Astrophys. J.*, 805(1):38, May 2015. doi: 10.1088/0004-637X/805/1/38.
- J. S. Dohnanyi. Collisional Model of Asteroids and Their Debris. *J. Geophys. Res.*, 74: 2531–2554, May 1969. doi: 10.1029/JB074i010p02531.

- C. Dominik and G. Decin. Age Dependence of the Vega Phenomenon: Theory. *Astrophys. J.*, 598(1):626–635, November 2003. doi: 10.1086/379169.
- J. Dorschner, B. Begemann, T. Henning, C. Jaeger, and H. Mutschke. Steps toward interstellar silicate mineralogy. II. Study of Mg-Fe-silicate glasses of variable composition. *Astron. Astrophys.*, 300:503, Aug 1995.
- C. P. Dullemond, A. Juhasz, A. Pohl, F. Sereshti, R. Shetty, T. Peters, B. Commercon, and M. Flock. RADMC-3D: A multi-purpose radiative transfer tool. *Astrophysics Source Code Library*, record ascl:1202.015, February 2012.
- D. Fedele, M. Carney, M. R. Hogerheijde, C. Walsh, A. Miotello, P. Klaassen, S. Bruderer, Th. Henning, and E. F. van Dishoeck. ALMA unveils rings and gaps in the protoplanetary system HD 169142: signatures of two giant protoplanets. *Astron. Astrophys.*, 600:A72, April 2017. doi: 10.1051/0004-6361/201629860.
- András Gáspár, Dimitrios Psaltis, George H. Rieke, and Feryal Özel. Modeling Collisional Cascades in Debris Disks: Steep Dust-size Distributions. *Astrophys. J.*, 754(1):74, July 2012. doi: 10.1088/0004-637X/754/1/74.
- Jane S. Greaves. Disks Around Stars and the Growth of Planetary Systems. *Science*, 307(5706):68–71, January 2005. doi: 10.1126/science.1101979.
- B. P. Kondratyev. Two-dimensional generalization of Gaussian rings and dynamics of the central regions of flat galaxies. *Mon. Not. Roy. Astron. Soc.*, 442(2):1755–1766, August 2014. doi: 10.1093/mnras/stu841.
- A. V. Krivov, I. Mann, and N. A. Krivova. Size distributions of dust in circumstellar debris discs. *Astron. Astrophys.*, 362:1127–1137, October 2000.
- A. V. Krivov, T. Löhne, and M. Sremčević. Dust distributions in debris disks: effects of gravity, radiation pressure and collisions. *Astron. Astrophys.*, 455(2):509–519, August 2006. doi: 10.1051/0004-6361:20064907.
- Alexander V. Krivov. Debris disks: seeing dust, thinking of planetesimals and planets. *Research in Astronomy and Astrophysics*, 10(5):383–414, May 2010. doi: 10.1088/1674-4527/10/5/001.

- Marc J. Kuchner and Matthew J. Holman. The Geometry of Resonant Signatures in Debris Disks with Planets. *Astrophys. J.*, 588(2):1110–1120, May 2003. doi: 10.1086/374213.
- Torsten Löhne, Alexander V. Krivov, and Jens Rodmann. Long-Term Collisional Evolution of Debris Disks. *Astrophys. J.*, 673(2):1123–1137, February 2008. doi: 10.1086/524840.
- Ryan A. Loomis, Karin I. Öberg, Sean M. Andrews, and Meredith A. MacGregor. A Multi-ringed, Modestly Inclined Protoplanetary Disk around AA Tau. *Astrophys. J.*, 840(1):23, May 2017. doi: 10.3847/1538-4357/aa6c63.
- V.N. L’vov, R.I. Smehacheva, C.C. Smirnov, and C.D. Tsekmejster. Some features of the movement of asteroids of the Hilda group. *Izvestiya GAO RAS*, 217:318–324, 2004.
- Sebastian Marino. Planetesimal/Debris discs. *arXiv e-prints*, art. arXiv:2202.03053, February 2022. doi: 10.48550/arXiv.2202.03053.
- Gustav Mie. Beiträge zur Optik trüber Medien, speziell kolloidaler Metallösungen. *Annalen der Physik*, 330(3):377–445, January 1908. doi: 10.1002/andp.19083300302.
- Sarah Morrison and Renu Malhotra. Planetary Chaotic Zone Clearing: Destinations and Timescales. *Astrophys. J.*, 799(1):41, January 2015. doi: 10.1088/0004-637X/799/1/41.
- Carl D. Murray and Stanley F. Dermott. *Solar System Dynamics*. 2000. doi: 10.1017/CBO9781139174817.
- Alexander J. Mustill and Mark C. Wyatt. Dependence of a planet’s chaotic zone on particle eccentricity: the shape of debris disc inner edges. *Mon. Not. Roy. Astron. Soc.*, 419(4): 3074–3080, February 2012. doi: 10.1111/j.1365-2966.2011.19948.x.
- Leonid M. Ozernoy, Nick N. Gorkavyi, John C. Mather, and Tanya A. Taidakova. Signatures of Exosolar Planets in Dust Debris Disks. *Astrophys. J.*, 537(2):L147–L151, July 2000. doi: 10.1086/312779.
- Tim D. Pearce and Mark C. Wyatt. Dynamical evolution of an eccentric planet and a less massive debris disc. *Mon. Not. Roy. Astron. Soc.*, 443(3):2541–2560, September 2014. doi: 10.1093/mnras/stu1302.
- Dirk Petry and CASA Development Team. Analysing ALMA Data with CASA. In P. Ballester, D. Egret, and N. P. F. Lorente, editors, *Astronomical Data Analysis Soft-*

ware and Systems XXI, volume 461 of *Astronomical Society of the Pacific Conference Series*, page 849, September 2012. doi: 10.48550/arXiv.1201.3454.

E. V. Pitjeva and N. P. Pitjev. Masses of the Main Asteroid Belt and the Kuiper Belt from the Motions of Planets and Spacecraft. *Astronomy Letters*, 44(8-9):554–566, August 2018a. doi: 10.1134/S1063773718090050.

E. V. Pitjeva and N. P. Pitjev. Mass of the Kuiper belt. *Celestial Mechanics and Dynamical Astronomy*, 130(9):57, September 2018b. doi: 10.1007/s10569-018-9853-5.

William H. Press, Saul A. Teukolsky, William T. Vetterling, and Brian P. Flannery. *Numerical recipes in C. The art of scientific computing*. Cambridge Univ. Press, Cambridge, 1992.

A. C. Quillen and Stephen Thorndike. Structure in the Epsilon Eridani Dusty Disk Caused by Mean Motion Resonances with a 0.3 Eccentricity Planet at Periastron. *Astrophys. J.*, 578(2):L149–L152, October 2002. doi: 10.1086/344708.

Alice C. Quillen. Predictions for a planet just inside Fomalhaut’s eccentric ring. *Mon. Not. Roy. Astron. Soc.*, 372(1):L14–L18, October 2006. doi: 10.1111/j.1745-3933.2006.00216.x.

Alice C. Quillen and Peter Faber. Chaotic zone boundary for low free eccentricity particles near an eccentric planet. *Mon. Not. Roy. Astron. Soc.*, 373(3):1245–1250, December 2006. doi: 10.1111/j.1365-2966.2006.11122.x.

Timothy J. Rodigas, Renu Malhotra, and Philip M. Hinz. Predictions for Shepherd Planets in Scattered Light Images of Debris Disks. *Astrophys. J.*, 780(1):65, January 2014. doi: 10.1088/0004-637X/780/1/65.

Jan Philipp Ruge, Sebastian Wolf, Tatiana Demidova, and Vladimir Grinin. Structures in circumbinary disks: Prospects for observability. *Astron. Astrophys.*, 579:A110, July 2015. doi: 10.1051/0004-6361/201321770.

G.I. Savin, B.M. Shabanov, P.N. Telegin, and A.V. Baranov. Joint Supercomputer Center of the Russian Academy of Sciences: Present and Future. *Lobachevskii Journal of Mathematics*, 40:1853–1862, November 2019. doi: 10.1134/S1995080219110271.

- Ivan I. Shevchenko. *Dynamical Chaos in Planetary Systems*, volume 463. 2020. doi: 10.1007/978-3-030-52144-8.
- J. Stoer and R. Bulirsch. *Introduction to Numerical Analysis*. Springer-Verlag, New York, 1980. doi: 10.1007/978-0-387-21738-3.
- Kate Y. L. Su, George H. Rieke, Renu Malhotra, Karl R. Stapelfeldt, A. Meredith Hughes, Amy Bonsor, David J. Wilner, Zoltan Balog, Dan M. Watson, Michael W. Werner, and Karl A. Misselt. Asteroid Belts in Debris Disk Twins: Vega and Fomalhaut. *Astrophys. J.*, 763(2):118, February 2013. doi: 10.1088/0004-637X/763/2/118.
- S. R. Taylor. On the Difficulties of Making Earth-Like Planets. *Meteoritics and Planetary Science Supplement*, 33:A153, July 1998.
- P. Thébault and J. C. Augereau. Collisional processes and size distribution in spatially extended debris discs. *Astron. Astrophys.*, 472(1):169–185, September 2007. doi: 10.1051/0004-6361:20077709.
- G. van der Plas, C. M. Wright, F. Ménard, S. Casassus, H. Canovas, C. Pinte, S. T. Maddison, K. Maaskant, H. Avenhaus, L. Cieza, S. Perez, and C. Ubach. Cavity and other radial substructures in the disk around HD 97048. *Astron. Astrophys.*, 597:A32, January 2017. doi: 10.1051/0004-6361/201629523.
- M. C. Wyatt. Evolution of debris disks. *Ann. Rev. Astron. Astrophys.*, 46:339–383, September 2008. doi: 10.1146/annurev.astro.45.051806.110525.
- M. C. Wyatt, S. F. Dermott, C. M. Telesco, R. S. Fisher, K. Grogan, E. K. Holmes, and R. K. Piña. How Observations of Circumstellar Disk Asymmetries Can Reveal Hidden Planets: Pericenter Glow and Its Application to the HR 4796 Disk. *Astrophys. J.*, 527(2):918–944, December 1999. doi: 10.1086/308093.
- M. C. Wyatt, R. Smith, J. S. Greaves, C. A. Beichman, G. Bryden, and C. M. Lisse. Transience of Hot Dust around Sun-like Stars. *Astrophys. J.*, 658(1):569–583, March 2007. doi: 10.1086/510999.

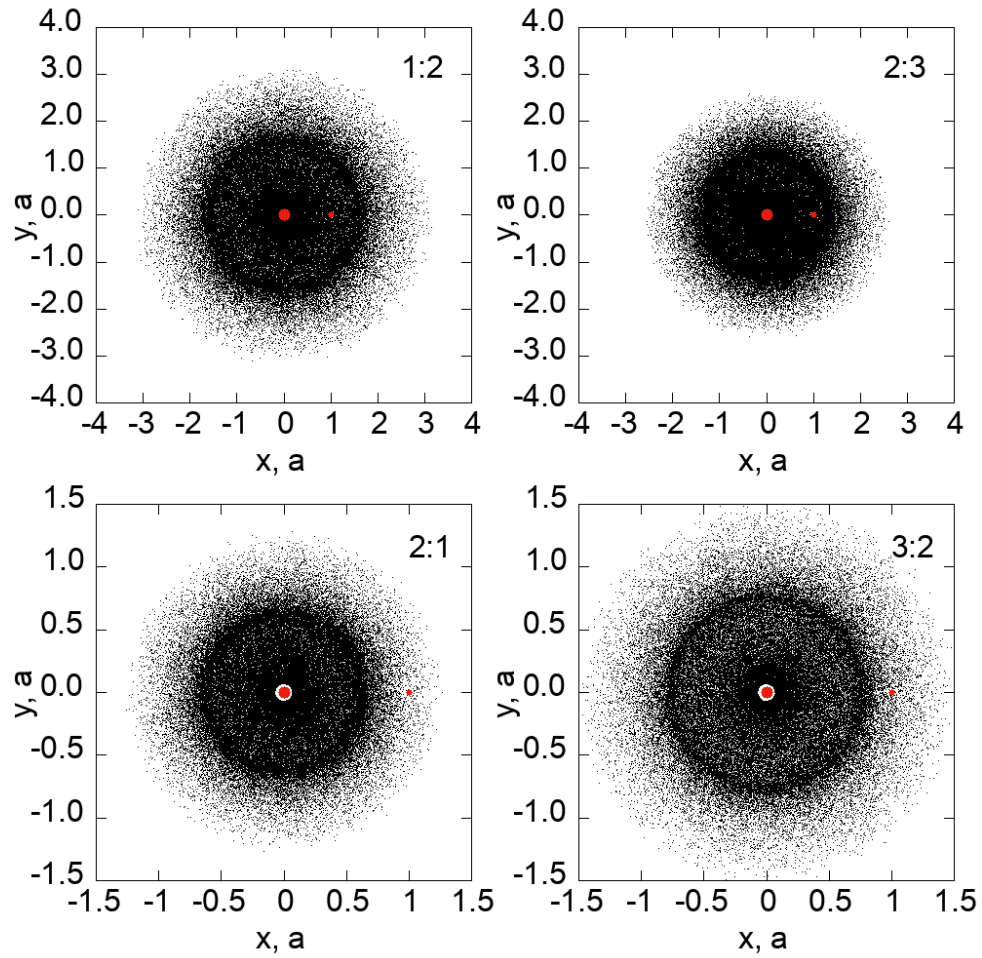


Figure 1: The initial ($t = 0$) distribution of particles at mean-motion resonances 1:2, 2:3, 2:1, and 3:2, in a model with the mass parameter $\lg \mu = -3$. The locations of the star and planet are marked with red dots. The coordinates along the axes are given in units of the semimajor axis of the planet's orbit.

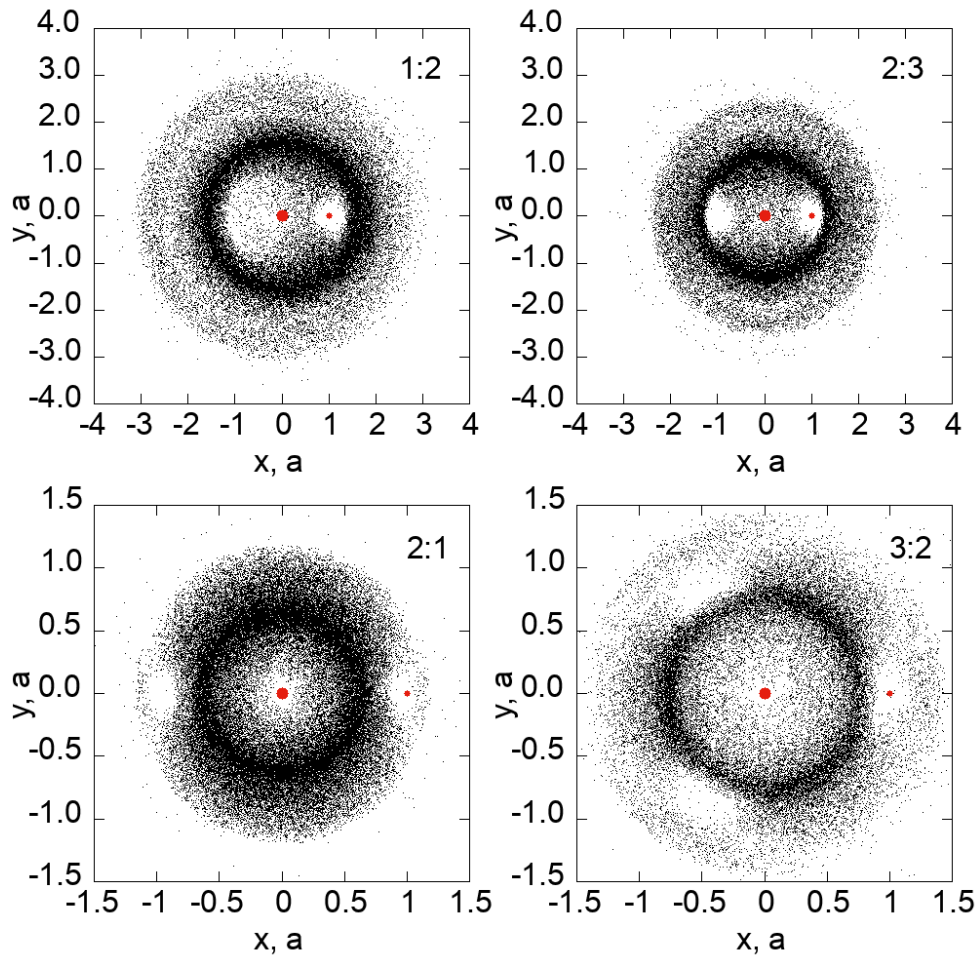


Figure 2: Same as Fig. 1, but at time $t = 10^5 P$.

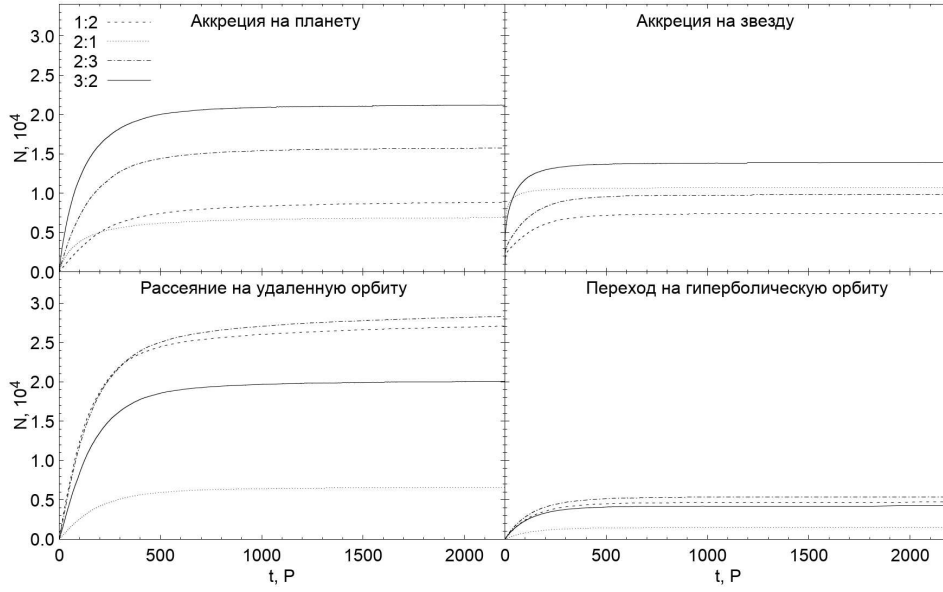


Figure 3: Number N of particles escaping (leaving the system) over time t : due to accretion onto the planet (upper-left), due to accretion onto the star (upper-right), scattering to distant orbits (lower-left), transition to hyperbolic orbits (lower-right); the mass parameter $\lg \mu = -3$ in all cases. The curves correspond to the dependences for particles initially distributed in zones of resonances 1:2 (dashed), 2:1 (dotted), 2:3 (dash-dotted), and 3:2 (solid). The number of particles is given in 10^4 units, and time is in the planet’s orbital periods.

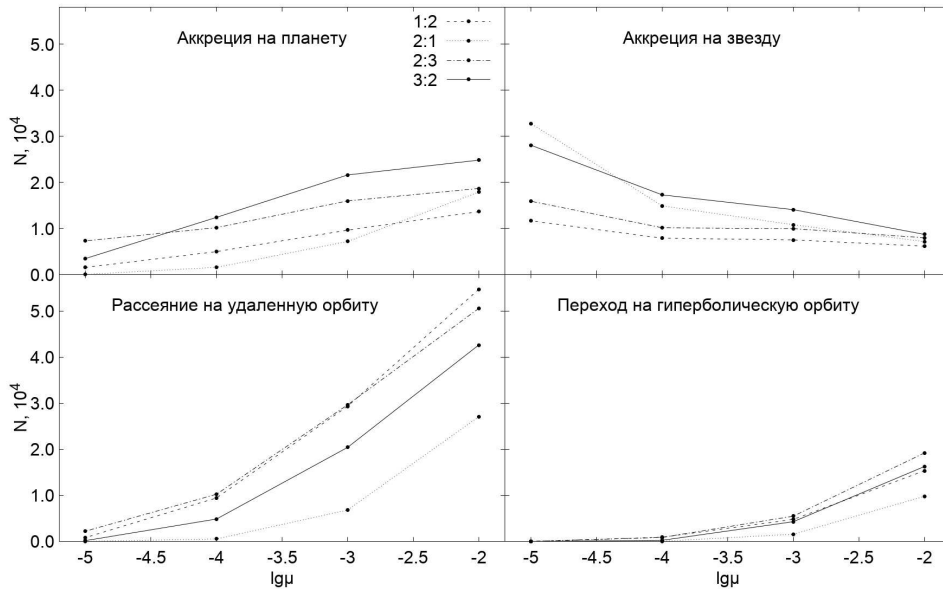


Figure 4: Number N of particles escaping over time $t = 10^5 P$, in dependence on the mass parameter μ : due to accretion onto the planet (upper-left), accretion onto the star (upper-right), scattering to distant orbits (lower-left), transition to hyperbolic orbits (lower-right). As in the previous Figure, the curves correspond to the dependences for particles initially distributed in zones of resonances 1:2 (dashed), 2:1 (dotted), 2:3 (dash-dotted), and 3:2 (solid). The number of particles is given in 10^4 units.

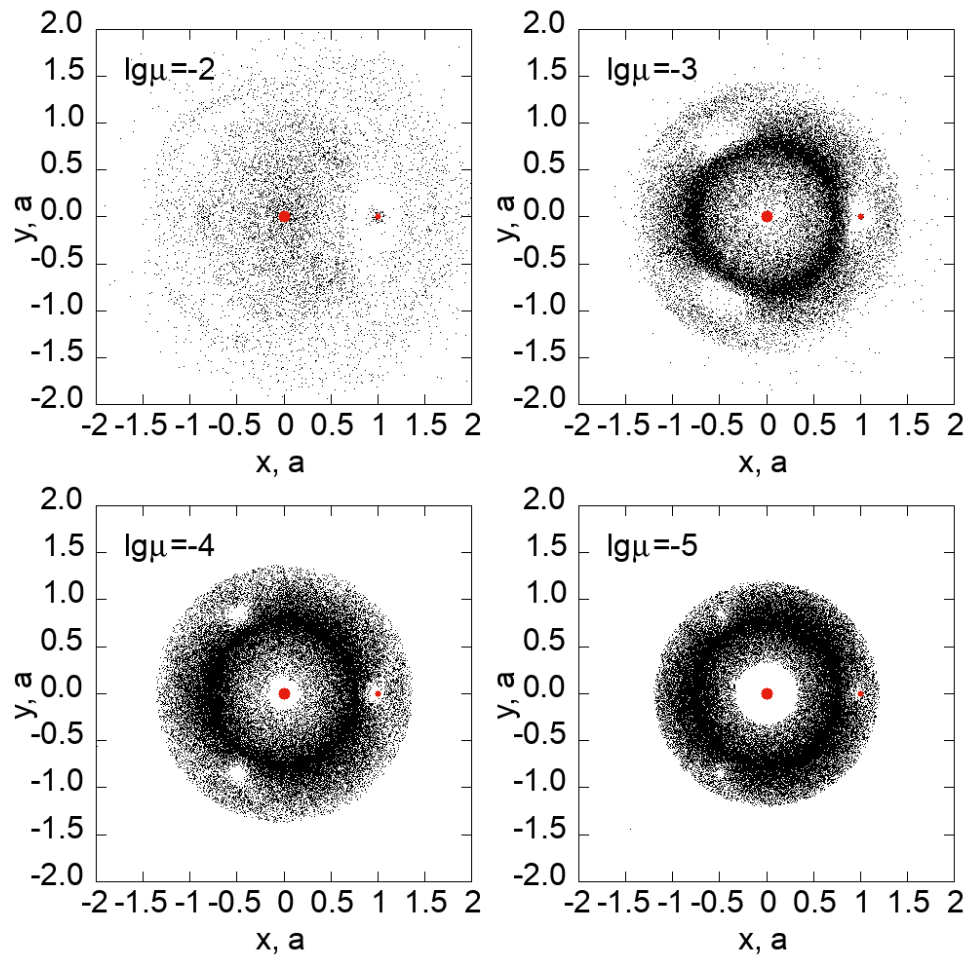


Figure 5: Same as Fig. 2, but for resonance 3:2; in models with the mass parameter $\lg \mu = -2$ (upper-left), $\lg \mu = -3$ (upper-right), $\lg \mu = -4$ (lower-left), and $\lg \mu = -5$ (lower-right).

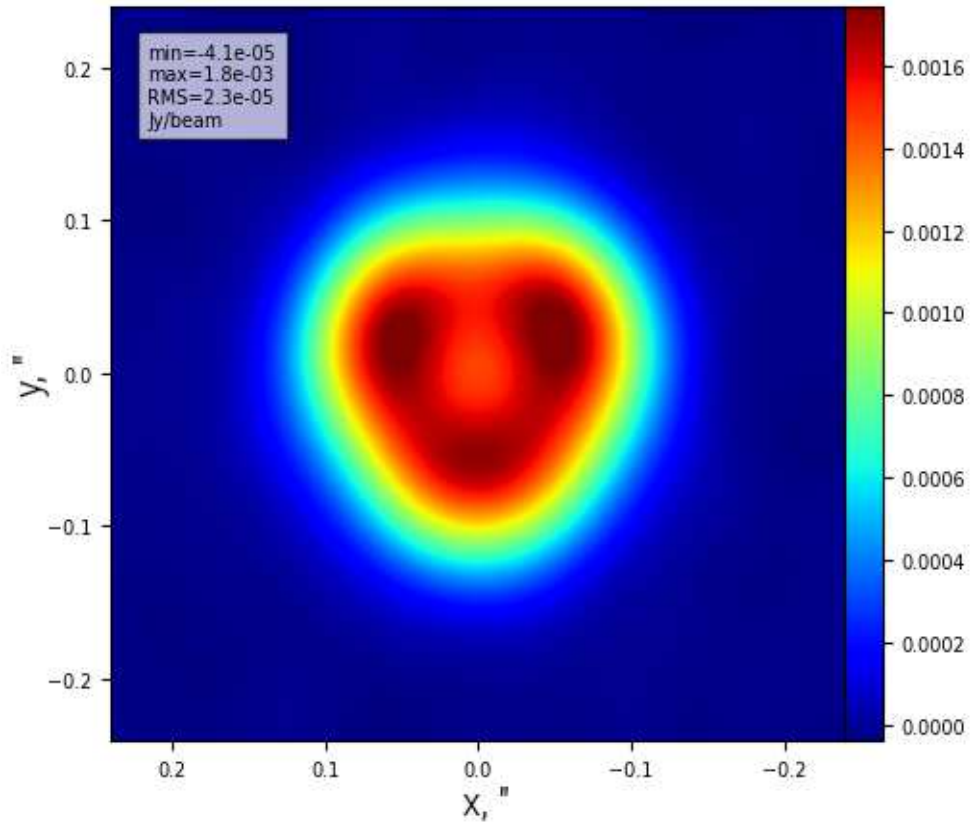


Figure 6: The debris disk image at wavelength $870 \mu\text{m}$ in the model with $a = 1 \text{ AU}$, $d = 10 \text{ pc}$, and $M_{\text{dust}} = 0.001M_{\oplus}$. The color scale is given in Jy/beam ; its maximum and minimum, as well as the signal-to-noise ratio, are indicated in the upper-left corner. The axial coordinates are given in arcseconds.

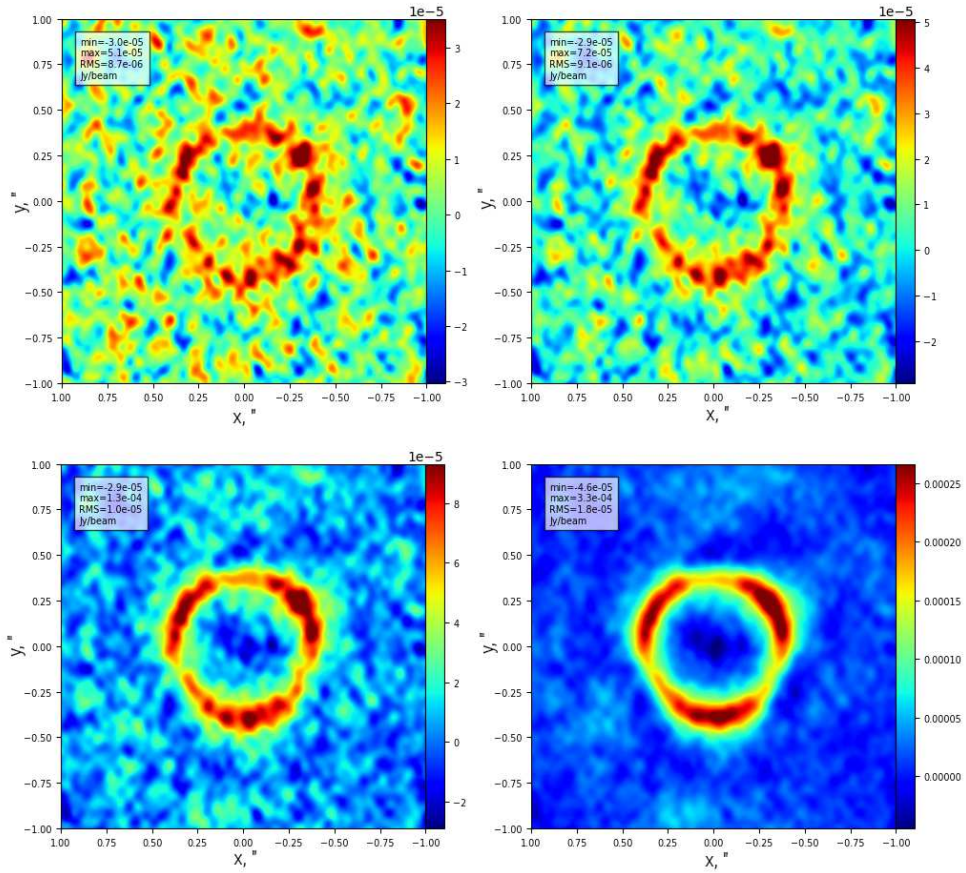


Figure 7: Same as Fig. 6, but in the models with $a = 5$ au and $d = 10$ pc; $M_{\text{dust}} = 0.0003 M_{\oplus}$ (upper-left), $M_{\text{dust}} = 0.005 M_{\oplus}$ (upper-right), $M_{\text{dust}} = 0.001 M_{\oplus}$ (lower-left), and $M_{\text{dust}} = 0.003 M_{\oplus}$ (lower-right).

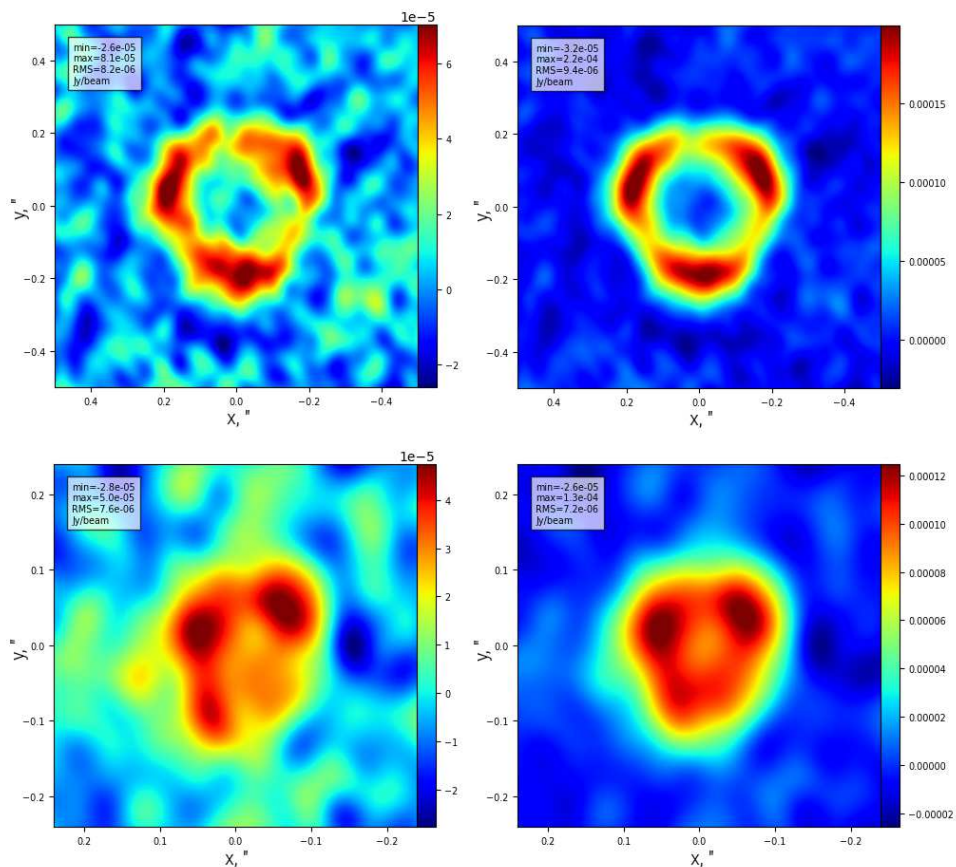


Figure 8: Same as in Fig. 6, but in the models with $a = 5$ au. The left-hand panels correspond to the models with $M_{\text{dust}} = 0.001 M_{\oplus}$, and the right-hand ones to those with $M_{\text{dust}} = 0.003 M_{\oplus}$. The observer-object distance $d = 20$ pc (upper panels) and $d = 50$ pc (lower panels).